minerals

MDPI

Article

Comparative Analysis of Reduction Techniques Aiming for the Minimization of Contaminated Soil with Red Mud

Srećko Stopić [1,*], Duško Kostić [1,2], Mitar Perušić [2], Richard Schneider [1], Isnaldi R. Souza Filho [3,4], Aleksandar Mitrašinović [5] and Bernd Friedrich [1]

[1] IME Process Metallurgy and Metal Recycling, RWTH Aachen University, 52056 Aachen, Germany; dkostic@ime-aachen.de (D.K.); bfriedrich@ime-aachen.de (B.F.)
[2] Faculty of Technology Zvornik, University of East Sarajevo, 75400 Zvornik, Republic of Srpska, Bosnia and Herzegovina; mitar.perusic@tfzv.ues.rs.ba
[3] Max-Planck-Institut for Sustainable Materials, Max-Planck-Strasse 1, 40237 Duesseldorf, Germany
[4] Institut Jean Lamour, CNRS (UMR 7198), Université de Lorraine, F-54000 Nancy, France
[5] Institute of Technical Sciences of the Serbian Academy of Sciences and Arts, 11000 Belgrade, Serbia; aleksandar.mitrasinovic@itn.sanu.ac.rs
* Correspondence: sstopic@ime-aachen.de

Abstract: Comparative analysis of red mud reduction techniques was performed using both carbothermal and hydrogen-based reduction methods, combining thermochemical modeling and experimental validation. The reduction process is mostly important because of the high contamination risk assessment of soil with disposed red mud. Therefore, the minimization of red mud during the reduction process can be a novel strategy for the production of metallic iron and solid residue for hydrometallurgical treatment. Different strategies of hydrogen and carbon reduction in static and dynamic conditions were studied between 700 °C and 1700 °C. The separation of solid residue and formed iron was analyzed using magnetic separation. The main aim was to study the advantages and disadvantages of using decarbonizing technologies for the treatment of red mud, aiming to develop an environmentally friendly process. Thermochemical analysis of the reduction offered new data about mass losses during our process through the evaporation, thermal decomposition, and formation of metallic carbide.

Keywords: reduction; red mud; hydrogen; carbon

check for updates

Academic Editor: Anthimos Xenidis

Received: 28 March 2025
Revised: 21 April 2025
Accepted: 29 April 2025
Published: 30 April 2025

Citation: Stopić, S.; Kostić, D.; Perušić, M.; Schneider, R.; Souza Filho, I.R.; Mitrašinović, A.; Friedrich, B. Comparative Analysis of Reduction Techniques Aiming for the Minimization of Contaminated Soil with Red Mud. *Minerals* **2025**, *15*, 470. https://doi.org/10.3390/min15050470

Copyright: © 2025 by the authors. Licensee MDPI, Basel, Switzerland. This article is an open access article distributed under the terms and conditions of the Creative Commons Attribution (CC BY) license (https://creativecommons.org/licenses/by/4.0/).

1. Introduction

The reduction of iron oxides is a fundamental process in metallurgy, particularly in the production of iron and steel. It involves the removal of oxygen from iron oxides, such as hematite (Fe_2O_3), magnetite (Fe_3O_4), and wüstite (FeO), to obtain metallic iron. This transformation is typically achieved through chemical reactions with reducing agents like carbon, carbon monoxide, or hydrogen [1].

In industrial settings, the most common method is the blast furnace process, where iron ore is reduced using coke at high temperatures, producing molten iron that is later refined into steel. An alternative approach, known as direct reduction, employs natural gas or hydrogen to convert iron oxides into solid sponge iron at lower temperatures. Hydrogen plasma reduction is another promising method that uses ionized hydrogen gas to achieve reduction at high efficiency and with minimal carbon emissions. Additionally, red mud, a byproduct of aluminum production rich in iron oxides, can be processed through reduction techniques to extract iron, making use of industrial waste. There is also

the thermite process, which uses aluminum to reduce iron oxide in a highly exothermic reaction [1–4].

- Carbothermic reduction

Carbothermic reduction is the primary method for extracting metals from ores using carbon as a reducing agent, playing a crucial role in iron and steel production. This process involves the reaction of iron oxides, such as hematite (Fe_2O_3) and magnetite (Fe_3O_4), with carbon (coke or charcoal) at high temperatures, typically in a blast furnace around 1500 °C. As carbon removes oxygen from the ore, it forms carbon monoxide (CO), which also reacts with iron oxides, producing carbon dioxide (CO_2) and metallic iron [5,6].

The choice of reduction method depends on factors such as energy efficiency, cost, and environmental impact. With increasing concerns about carbon emissions, newer techniques focusing on hydrogen-based reduction, hydrogen plasma, and carbon-neutral approaches are being explored to make the process more sustainable for the future of iron and steel production.

$$3Fe_2O_3 + CO \rightarrow 2Fe_3O_4 + CO_2 \quad (1)$$

Then, magnetite is reduced to wüstite (FeO) [6] as follows:

$$Fe_3O_4 + CO \rightarrow 3FeO + CO_2 \quad (2)$$

Finally, wüstite (FeO) is reduced to metallic iron [6] as follows:

$$FeO + CO \rightarrow Fe + CO_2 \quad (3)$$

Carbothermic reduction is an endothermic process requiring energy, which is supplied by carbon combustion in the presence of oxygen. This generates carbon monoxide, which, along with coke, acts as a reducing agent, forming the basis of pig iron production. Pig iron contains carbon and impurities, necessitating further refining for pure steel. A similar process applies to red mud, as it contains iron (III) oxide, like iron ore. Efficiency depends on factors such as carbon reactivity, furnace temperature and pressure, and ore characteristics. Optimal conditions ensure complete reduction while minimizing slag formation. Thermodynamically, Gibbs free energy favors a reduction of metallic oxides at higher temperatures, while reaction kinetics influence overall efficiency [7–9].

- Hydrogen reduction

Carbon remains the dominant reducing agent in global metal production, with carbothermic reduction considered the most cost-effective method. However, the industry is under pressure to reduce carbon emissions, and hydrogen is emerging as a promising alternative. The European Union aims to cut industrial carbon emissions by up to 95% by 2050, while Australia is actively promoting hydrogen as a long-term solution, with initiatives like the Hydrogen Working Group supporting clean hydrogen adoption by 2030 [10].

Hydrogen offers significant environmental benefits, reducing CO_2 emissions by up to 95%, with water as its only byproduct. However, its high production costs, energy-intensive generation (especially for green hydrogen), and safety concerns pose major challenges. Large-scale adoption requires significant expansion in production capacity, as well as advancements in storage and transport. Currently, less than 10% of global hydrogen is used in metal production, mainly for refractory metal powders like tungsten, molybdenum, and some iron and nickel [11].

The reduction of hematite by hydrogen proceeds in two or three steps, via magnetite (Fe_3O_4) and wüstite (FeO), according to the following equations [3]:

$$3Fe_2O_3 + H_2 \rightarrow 2Fe_3O_4 + H_2O \quad (4)$$

$$Fe_3O_4 + H_2 \rightarrow 3FeO + H_2O \quad (5)$$

$$FeO + H_2 \rightarrow Fe + H_2O \quad (6)$$

Despite its potential, hydrogen reduction faces industrial limitations. Its weaker reducing ability compared to carbon at high temperatures, the endothermic nature of the process, and the need for reactor redesigns complicate large-scale implementation. Additionally, hydrogen interactions with impurities can affect efficiency, while high operational costs remain a barrier to widespread adoption [12].

- Hydrogen plasma reduction

In addition to direct hydrogen reduction, an innovative approach involves using plasma hydrogen to reduce metallic oxides. Plasma hydrogen provides kinetic and thermodynamic advantages due to its highly reactive ionic and vibrationally excited species, which transfer energy efficiently to alter raw material structures. This localized heating reduces the need for bulk heating, improving overall energy efficiency [13].

Plasma, the fourth state of matter, forms when high energy ionizes a gas. Industrial plasmas are classified as thermal and non-thermal, with thermal plasmas generated through electrode discharge, radiofrequency, or microwave fields at very low pressures. High electron temperatures and rapid collisions among species enable quick local thermodynamic equilibrium, making plasma hydrogen a promising alternative for metal reduction [13].

Hydrogen plasma reduction is an advanced metallurgical technique for reducing iron oxides, mainly hematite, into metallic iron. Plasma is created by supplying high energy to hydrogen gas, often mixed with argon, ionizing hydrogen molecules through electrical discharge, radiofrequency, or microwave fields. This generates a reactive plasma containing ions (H^+), electrons, atomic hydrogen (H), and excited molecular species, like H_2* and H_3^+ [14].

When hematite (Fe_2O_3) interacts with hydrogen plasma, its high-energy components initiate reduction. Highly reactive atomic hydrogen and hydrogen ions first convert hematite to magnetite (Fe_3O_4), marking the initial step in the reduction process [15] as follows:

$$3Fe_2O_3 + 2H \rightarrow 2Fe_3O_4 + H_2O \quad (7)$$

and then a reduction of magnetite to wüstite

$$Fe_3O_4 + 2H \rightarrow 3FeO + H_2O \quad (8)$$

and finally, to metallic iron (Fe)

$$FeO + 2H \rightarrow Fe + H_2O \quad (9)$$

Hydrogen plasma reduction offers advantages over conventional hydrogen and carbon-based methods, including localized heating for better energy efficiency and faster reduction due to highly reactive plasma species. It also produces only water vapor, making it environmentally friendly compared to carbothermic reduction [14].

However, challenges include maintaining stable plasma conditions, controlling energy input, and preventing unwanted reactions. Optimizing temperature, pressure, and plasma composition is essential for efficiency. Despite these hurdles, hydrogen plasma reduction

holds great potential for sustainable iron production, with future research focusing on scaling up and improving plasma generation for industrial applications [16].

- Red Mud

Red mud (RM), a byproduct of alumina production, is named for its red color due to its high iron oxide content. Typically, 0.5 to 2 tons of red mud are produced per ton of alumina, with global accumulation surpassing 5 billion tons by 2020, led by China. Red mud's complex composition includes CaO, SiO_2, Fe_2O_3, TiO_2, Na_2O, K_2O, and various minerals. Its high alkalinity (pH 9.0 to 13.2) is mainly due to soluble and insoluble alkalis, which can pose environmental threats like groundwater contamination, corrosion, and toxicity to organisms [17–19].

Safe disposal of red mud is a major challenge, with methods like slurry disposal, dry mud disposal, and solar drying being used. Red mud dams, designed to store large quantities of this material, help prevent leakage and control environmental risks. However, red mud's high alkalinity, potential heavy metal contamination, and fine particles pose significant environmental and health risks, such as soil and water pollution, corrosion, and air pollution. The Kolontar disaster in Hungary highlighted the catastrophic potential of improper red mud management, causing environmental damage, injuries, and loss of life. Proper management is crucial to mitigate these risks [20–23].

Thermochemical modeling has been conducted to analyze the reduction of red mud using both carbon and hydrogen as reducing agents. Red mud, a byproduct of the aluminum industry, contains a significant amount of iron oxides, making it a potential secondary source for iron extraction. The reduction process has been studied using FactSage 8.0, a powerful thermochemical software, to simulate reaction mechanisms, equilibrium compositions, and process efficiency under different conditions.

For carbon-based reduction, modeling evaluates how coke or charcoal interacts with iron oxides in red mud, examining temperature-dependent reaction pathways and the formation of byproducts, such as slag and CO_2. Similarly, hydrogen reduction modeling focuses on the efficiency of hydrogen gas in converting iron oxides to metallic iron, analyzing reaction kinetics, temperature influence, and the environmental benefits of water vapor as the only byproduct.

The novelty of this paper lies in the comprehensive analysis of various reduction methods for extracting iron from red mud, with a focus on carbon and hydrogen reduction in both tubular furnaces and rotary kilns, as well as hydrogen plasma reduction. This study not only explores conventional reduction methods but also introduces the potential of hydrogen plasma reduction, which is a more sustainable and energy-efficient approach. Furthermore, the paper employs advanced thermochemical modeling using FactSage to simulate and compare the reaction mechanisms, equilibrium compositions, and process efficiencies of these reduction methods under various conditions. By combining experimental approaches with detailed modeling, this paper provides valuable insights into optimizing reduction processes for red mud, offering a thorough comparison of traditional and innovative techniques for metal extraction, with particular attention to environmental impact and scalability.

2. Materials and Methods

Many advanced analytical techniques were employed to accurately characterize and analyze the materials involved in this research. Each of these methods provides distinct insights into the structure, composition, and size of the samples. Used techniques are X-ray diffraction (XRD-Bruker D8 Advance with LynxEye detector, Billerica, MA, USA), Energy-Dispersive X-ray Spectroscopy (EDS-Octane Plus-A detector by Ametek-EDAX, Berwyn, PA, USA), Scanning Electron Microscopy (SEM-JSM 7000F by JEOL (2006 model,

JEOL Ltd., Tokyo, Japan)), Inductively Coupled Plasma Optical Emission Spectroscopy (ICP-OES Agilent 5000, Santa Clara, CA, USA), RWTH, and Aachen.

In this work, red mud from the factory "Alumina" Ltd. Zvornik (Zvornik, Republic of Srpska, Bosnia and Herzegovina) was used as a raw material. The red mud is previously dried, grounded, and prepared for the reduction process. In Table 1, the chemical composition of the used red mud is shown.

Table 1. Composition of red mud from "Alumina" Ltd. Zvornik.

Compounds	Wt., %	Compounds	Wt., %
Ignition loss at 1000 °C	8.32	Ga_2O_3	0.225
SiO_2	10.52	CuO	0.007
Fe_2O_3	49.29	K_2O	0.159
Na_2O	2.45	Tl_2O_3	0.088
TiO_2	4.59	MnO	0.145
CaO	8.23	MgO	0.627
Al_2O_3	12.03	NiO	0.034
Ag_2O	0.001	PbO	0.019
BaO	0.014	P_2O_5	0.930
Cr_2O_3	0.133	ZnO	0.016
Sc_2O_3	0.011	V_2O_5	0.135
Co_2O_3	0.012	SrO	0.075

Red mud characterization was performed using ICP and EDS analysis.

The XRD analysis in Figure 1 has confirmed the presence of hematite and other very stable oxides for reduction, including ilmenite. Analysis shows that other non-ferrous minerals, such as perovskite, calcite, diaspore, boehmite, anhydrite, etc., will undergo structural change caused by iron oxide reduction.

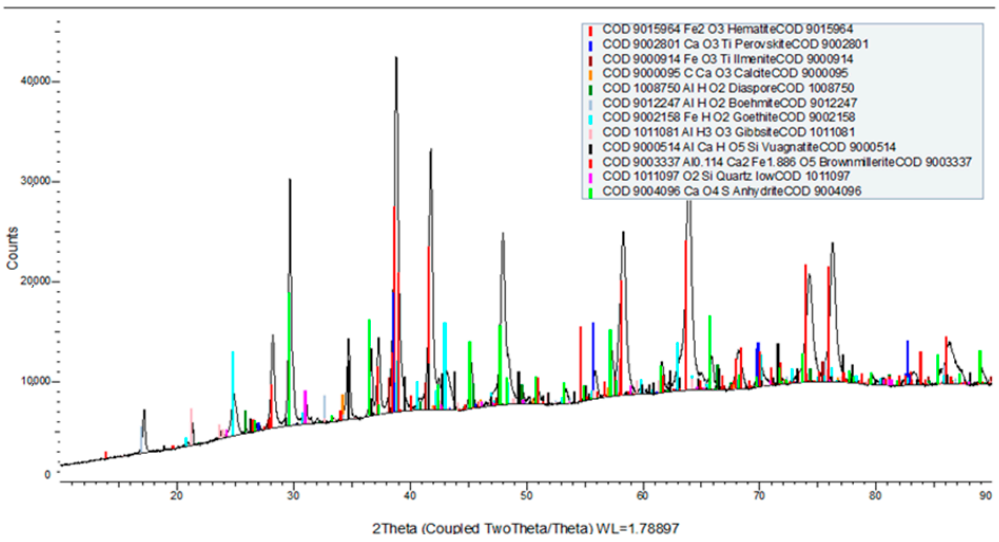


Figure 1. XRD analysis of red mud.

The reduction process with carbon took place in an electric arc furnace (carbothermal reduction), the reduction process with hydrogen was carried out in a tubular furnace (H-tubular reduction) and a rotary kiln (H-rotary kiln reduction), and hydrogen plasma

reduction was carried out at the Max Plank Institute for Sustainable Materials in Dusseldorf (H-plasma reduction). The reduced samples were separated mechanically using magnetic separation. The obtained products were analyzed by XRD and EDS analysis as well as SEM analysis. In Table 2, the design of the reduction experiments is shown.

Table 2. Design of the reduction experiments.

Exp. No	Reducing Agent	Temperature (°C)	Time (min)	Mass or Flow of Reducing Agent
1	Carbon (EAF)	1600	60	10 g
2	Hydrogen (rotary kiln)	920	120	2 L/min
3	Hydrogen (tubular furnace)	800	60	3 L/min (2 H_2/1Ar)
4	Hydrogen (tubular furnace)	900	60	3 L/min (2 H_2/1Ar)
5	Hydrogen (tubular furnace)	1000	60	3 L/min (2 H_2/1Ar)
6	Hydrogen plasma	2500	5	10 L/min (1 H_2/9Ar)
7	Hydrogen plasma	2500	10	10 L/min (1 H_2/9Ar)
8	Hydrogen plasma	2500	15	10 L/min (1 H_2/9Ar)

The reduction process with hydrogen as a reducing agent could not take place at a higher temperature due to equipment limitations. Hydrogen reduction equipment cannot withstand temperatures higher than 1000 °C.

2.1. Thermochemical Modeling

For the thermochemical analysis of the reduction of red mud at temperatures of 1600 °C and 1700 °C for different concentrations of both hydrogen and carbon, the calculation is performed without reducing agents. The thermodynamic modeling of the reduction of iron oxide from red mud is carried out using FactSage™ 8.0 software [24], developed by GTT Technologies, Kohlscheid, Germany. This modeling approach allows for a detailed analysis of phase equilibria and chemical reactions under varying conditions. The chemical composition of red mud used for calculations is a SiO_2 content of 12.43%. Iron oxide content is 58.22%, titanium dioxide content is 5.42%, calcium oxide is 9.72%, and alumina content is 14.21%.

A detailed overview of all input parameters and simulation conditions is presented in Table 3. In each simulation, a fixed input mass of 100 g of red mud is used to ensure consistency in comparative analysis.

Table 3. Design of the experiments for thermochemical modeling.

Experiment No.	Temperature (°C)	Mass of Reducing Agent (g)
1	1600 and 1700	0 (Hydrogen)
2	1600 and 1700	5 (Hydrogen)
3	1600 and 1700	10 (Hydrogen)
4	1600 and 1700	15 (Hydrogen)
5	1600 and 1700	20 (Hydrogen)
6	1600 and 1700	25 (Hydrogen)
7	1600 and 1700	30 (Hydrogen)
8	1600 and 1700	35 (Hydrogen)
9	1600 and 1700	40 (Hydrogen)

Table 3. *Cont.*

Experiment No.	Temperature (°C)	Mass of Reducing Agent (g)
10	1600 and 1700	45 (Hydrogen)
11	1600 and 1700	50 (Hydrogen)
12	1600 and 1700	0 (Carbon)
13	1600 and 1700	5 (Carbon)
14	1600 and 1700	10 (Carbon)
15	1600 and 1700	15 (Carbon)
16	1600 and 1700	20 (Carbon)

The simulations cover hydrogen and carbon at different concentrations to examine their effects on phase transformations, metal recovery rates, and byproduct formation.

2.2. Carbothermic Reduction in an Electric Arc Furnace

The particle sizes of red mud have values between 4.7 and 5.98 µm. The reduction process of red mud with carbon took place in a DC electric arc furnace at 1600 °C for 90 min. Three (3) kg of red mud and 10 g of graphite per 100 g of red mud as carbon-reducing agents are mixed and charged into the furnace. Because of the high viscosity of the slag after reducing the iron oxides, the slag creates a foam. To lower the viscosity, CaO has been added as a fluxing agent. We added 100 g CaO/3 kg red mud in order to facilitate the separation of slag and formed metallic iron. The positive side effect of CaO is that it is possible that FeO from Fe_2SiO_4 is dissolved back into the slag with a positive change in the activity of FeO. After charging, a holding time of 45 min has been started to let the C react with the slag. After the holding time, the furnace was tapped to extract the Fe metal phase, while the slag phase remained in the crucible. The samples were separated mechanically using magnetic separation [25].

2.3. Hydrogen Reduction in a Tubular Furnace

A reduction of 1.0 g of red mud was performed in a small tubular furnace at temperatures 800, 900, and 1000 °C for 60 min. According to previous studies of hydrogen reduction [26–30], the reduction process utilized a hydrogen flow rate of 2 L/min and an argon flow rate of 1 L/min [31].

2.4. Hydrogen Reduction in a Rotary Kiln

The reduction of red mud was conducted using a Carbolite rotary kiln. The objective was to investigate the reduction behavior of red mud in a controlled hydrogen atmosphere at high temperatures. A quartz tube was employed as the reaction chamber, and the process was carried out at 920 °C with hydrogen gas flows to facilitate controlled reduction. Figure 2 shows the equipment used for the experiments.

A total of 200 g of red mud was placed inside the quartz tube, which was then securely connected to the rotary kiln. Nitrogen gas was continuously supplied throughout the heating process. Once the system reached the target temperature of 920 °C, hydrogen was introduced at a flow rate of 1 L/min for 10 min, followed by another 10 min of minimal hydrogen flow.

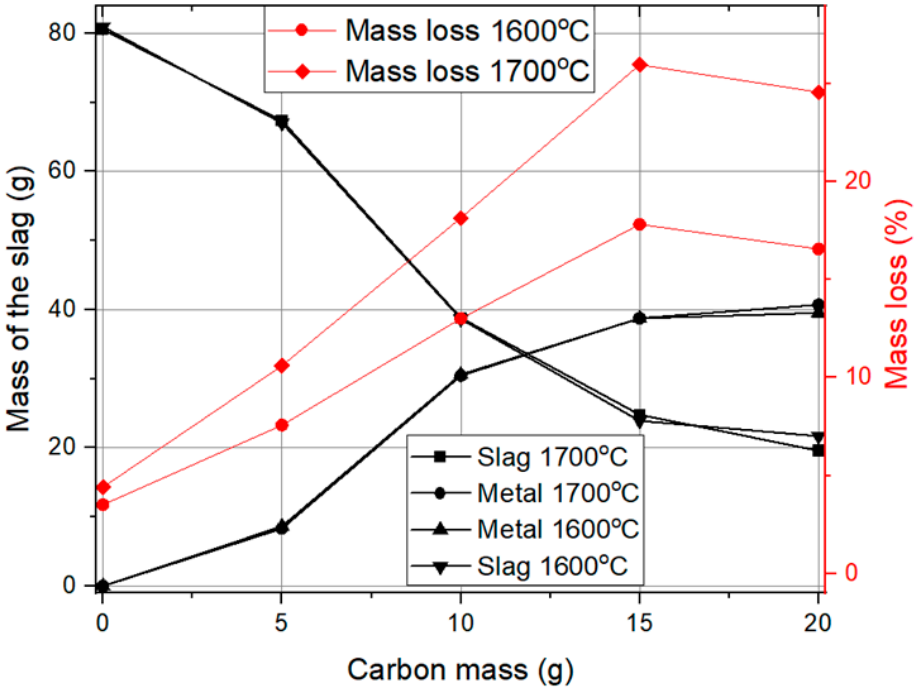


Figure 2. Mass loss and the mass of the slag and metal dependence on the carbon mass.

2.5. Hydrogen Plasma Reduction in an Electric Arc Furnace

The electric arc furnace is equipped with a tungsten electrode with a diameter of 6 mm. For the experiments, 20 g of red mud was placed into the water-cooled, copper sample holder. For the melting process, the 18-liter melting chamber is filled with a gas mixture consisting of 10% hydrogen and 90% argon. The total pressure is 900 mbar. An arc is ignited from the electrode to the red mud, which consists of plasma heated to 2350–2050 °C. The melting process is cyclical. Each cycle consists of melting the red mud with the plasma for one minute, followed by a brief cooling of the feed material. During the cooling phase, the hydrogen consumed during the reduction is replenished. The overall reduction time is evaluated.

The obtained products were analyzed by XRD, EDS analysis, and SEM analysis.

3. Results and Discussion

3.1. Carbothermal Reduction Modeling

During the reduction process, Fe_2O_3 is firstly reduced to FeO, and with the increase in reducing agent mass, it is further reduced to metallic Fe [32]. After the reduction process, there are two phases: slag, which is low in Fe, and the metal Fe phase. The carbothermal reduction of oxides from red mud was calculated and shown in Figure 2.

At 0 g of carbon mass, the process consists only of the decomposition of red mud at high temperatures, leading to the formation of slag without any metal phase. As the carbon mass increases, the metal content also increases, while the slag content decreases. This change is quite significant up to around 15 g of carbon mass, after which the variations are not as significant.

Regarding temperature effects, the trends in slag and metal mass are similar at both 1600 °C and 1700 °C. However, a slightly better metal yield is observed at 1700 °C, indicating a more efficient reduction process at higher temperatures. Mass loss trends show that higher temperatures result in greater mass loss, but the difference is not very significant. The overall observation suggests that increasing the carbon mass plays a crucial role in metal extraction, while temperature has a moderate but noticeable impact.

The Figure 3 illustrates the composition of alloying elements in iron during carbothermal reduction. At lower carbon mass values between 5 and 10 g, iron dominates with a content close to 100%. However, with an increase in carbon mass beyond 15 g, there is a significant rise in the content of other elements in the metal phase. Silicon content increases notably, reaching values up to 11%, while titanium and carbon contents also show substantial growth. The presence of carbon in the metal phase suggests an excess amount beyond what is needed for reduction. Temperature plays a significant role in this process, with higher carbon content leading to a greater incorporation of impurities. At 1700 °C, the content of all alloying elements in iron is higher compared to 1600 °C, indicating that increased temperature enhances impurity dissolution. This suggests that a carbon mass above 10 g leads to excessive impurity formation, which may not be desirable for obtaining high-purity iron.

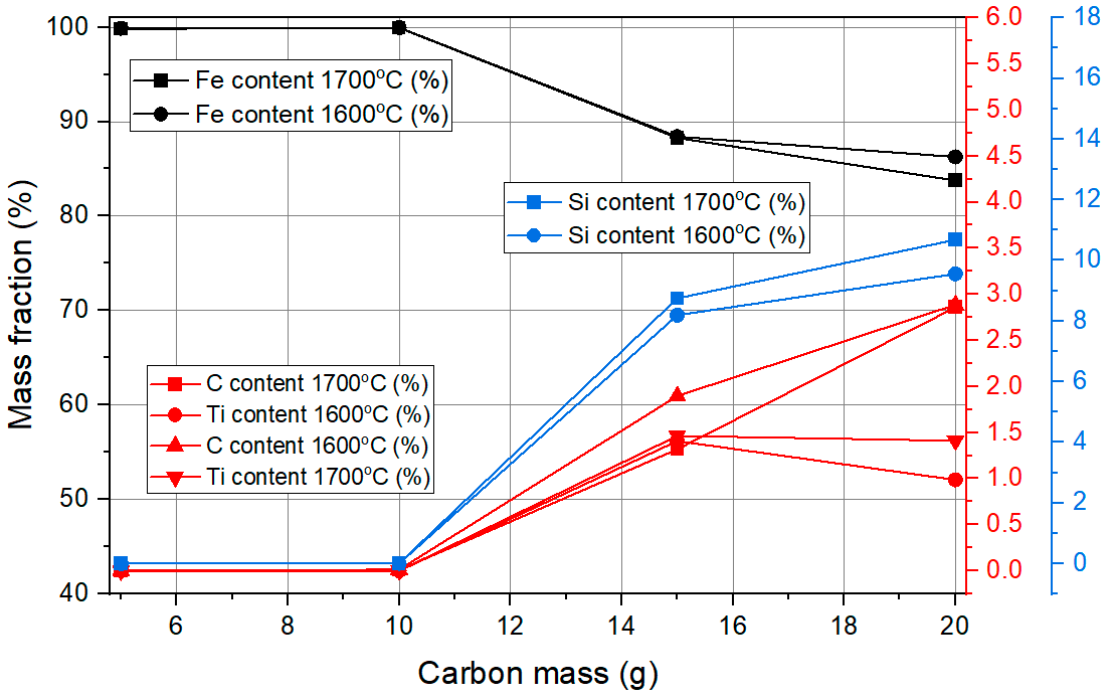


Figure 3. The mass fraction of elements in the metal phase correlates with the carbon mass.

Figure 4 shows the transformation of iron oxides with varying carbon masses and temperatures. The Fe_2O_3 content drops significantly with the addition of just 5 g of carbon, but it does not directly reduce to metallic iron. Instead, it first converts into FeO. The FeO content then decreases sharply as the carbon mass increases, reaching a very low level, close to zero, at around 15 g of carbon. This suggests that the reduction process occurs in stages, with Fe_2O_3 first reducing to FeO before eventually transforming into metallic iron. Additionally, at higher carbon masses, a third phase, TiC, is formed due to the excess carbon, indicating that beyond a certain point, surplus carbon leads to the formation of additional carbide phases instead of contributing to further iron reduction.

These observations suggest that the optimal carbon mass for achieving a high Fe content while minimizing excessive alloying and carbide formation lies between 10 g and 15 g. Beyond this range, further carbon additions promote carbide formation, which may influence the final properties of the metal phase.

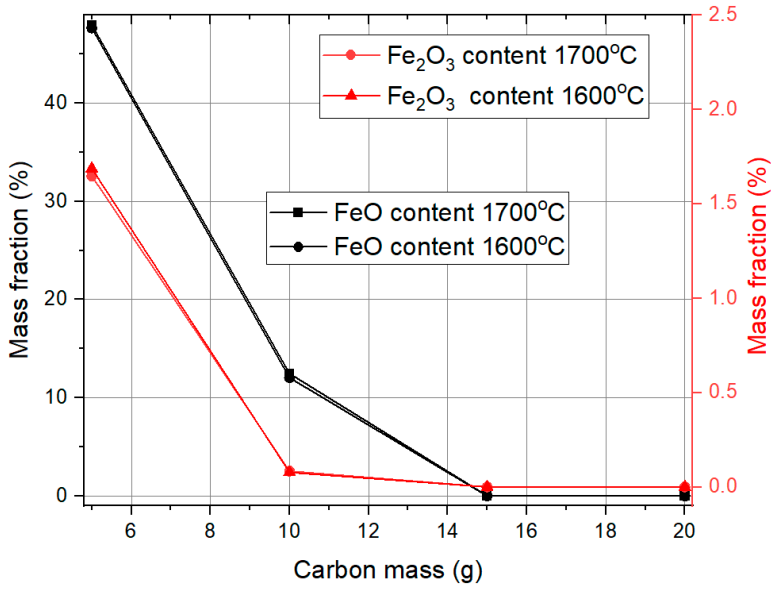


Figure 4. Mass fraction dependence on the carbon mass.

3.2. Hydrogen Reduction Modeling

The hydrogen reduction of oxides from red mud is calculated and shown in Figure 5.

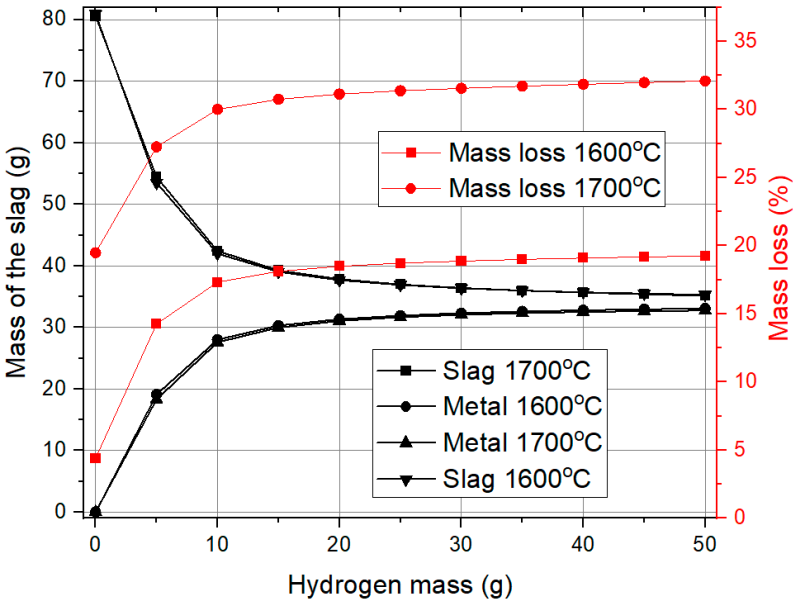


Figure 5. Mass loss and mass of the slag and metal dependence on the hydrogen mass.

Figure 5 shows the influence of hydrogen mass on slag mass and mass loss during the reduction process. Initially, with no hydrogen present, the system is entirely composed of red mud, resulting in the maximum slag mass. As hydrogen is introduced, reduction reactions take place, leading to a notable decrease in slag mass and a corresponding increase in metal formation. This effect is most significant for up to 20 g of hydrogen, beyond which additional hydrogen has little impact on further reducing the slag or increasing metal yield, proving that the reaction is almost complete.

Mass loss exhibits a similar pattern. With the hydrogen mass increase, oxygen from iron oxide reacts with hydrogen to form water vapor. Up to 20 g of hydrogen, mass loss increases significantly, but beyond this point, the effect becomes less significant, suggesting that most reducible oxides have already been removed. Temperature variation from 1600 °C

to 1700 °C does not greatly influence slag reduction or metal formation, but it does have a noticeable effect on mass loss. At 1700 °C, mass loss is higher, likely due to enhanced reaction rates and increased volatilization of reaction byproducts.

These findings suggest that 20 g of hydrogen is an optimal threshold for the reduction process. Beyond this, additional hydrogen offers minimal benefits in terms of metal recovery and slag reduction, while promoting slightly greater mass loss at higher temperatures.

Figure 6 presents how the mass fractions of different iron-containing species change with increasing hydrogen mass. The Fe_2O_3 content in the slag decreases sharply from 58% to nearly zero when the hydrogen mass reaches 5 g, indicating that Fe_2O_3 is rapidly reduced. However, this reduction also does not occur directly to metallic iron; instead, Fe_2O_3 first converts into FeO, which was not initially present in the red mud, similar to carbothermal reduction.

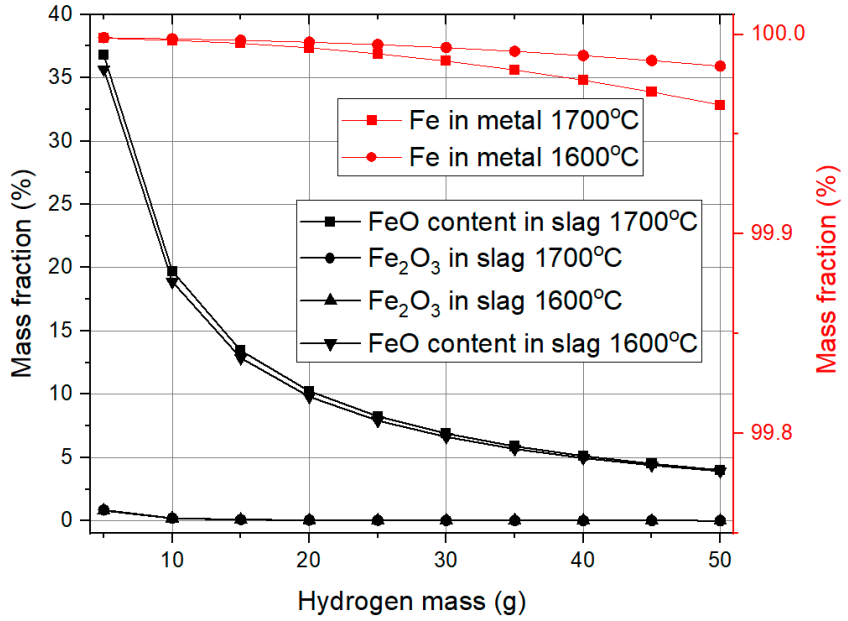


Figure 6. Mass fraction dependence on the hydrogen mass.

As hydrogen mass increases further, FeO content in the slag continues to decrease, reaching approximately 4% at 50 g of hydrogen. Beyond 25 g, the rate of decrease slows down, suggesting that most reducible iron oxides have already been converted into metallic iron. The iron content in the metal phase shows a slight decline as hydrogen mass increases, likely due to minor alloying with elements from the slag. However, this effect remains insignificant, as iron purity stays above 99.9%, demonstrating that the reduction process is highly effective in producing pure metallic iron.

Temperature variation from 1600 °C to 1700 °C does not have a major impact on the reduction process, except in the final iron content. At higher hydrogen masses, iron purity is slightly lower at 1700 °C than at 1600 °C, but the difference is negligible. An important observation is that hydrogen reduction produces significantly cleaner iron at all hydrogen mass levels compared to carbon reduction, highlighting its effectiveness in minimizing impurity incorporation. However, the efficiency of iron oxide reduction is slightly better for carbothermic reduction.

3.3. Carbothermic Reduction in an Electric Arc Furnace

In Figure 7, thermodynamic calculations of carbothermic and hydrogen reduction processes are compared to the experimentally obtained results.

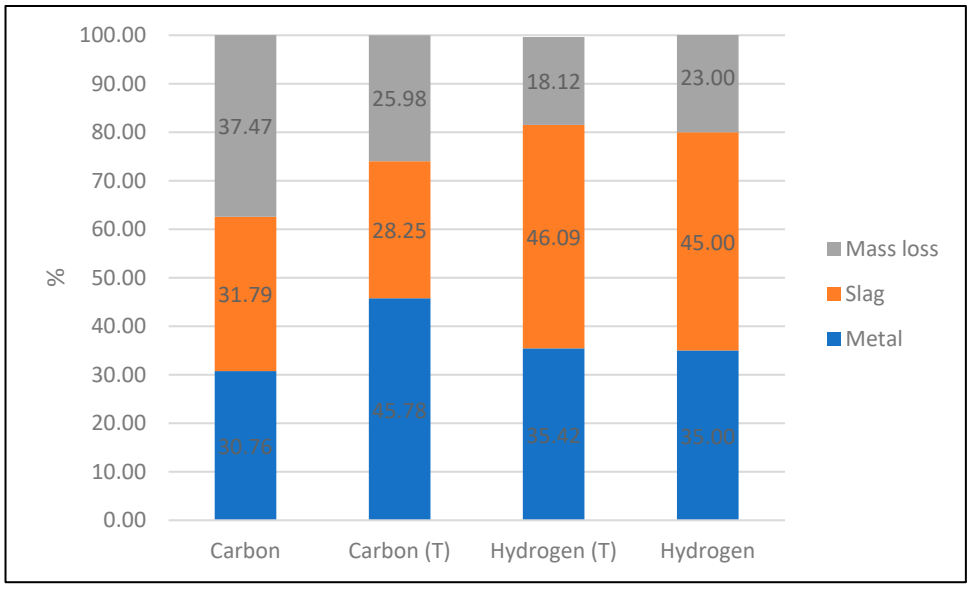


Figure 7. Thermodynamic calculation of the carbon and hydrogen reduction of red mud (T) and the experimentally obtained results.

Figure 7 shows the results comparison of the theoretically obtained results with the experimental results. It can be seen that there are slight variations, especially in carbothermic reduction, while for the hydrogen reduction process, theoretical and real experimental data are similar. Mass loss can be attributed to the reduction of oxygen from iron oxide (up to 15%) and evaporation in a neutral atmosphere (up to 9%). Particles obtained after hydrogen and carbothermic reduction exhibited magnetic properties, which are crucial for the separation process. ICP is used for elemental analysis of the carbothermic-reduced slag, as shown in Figure 8.

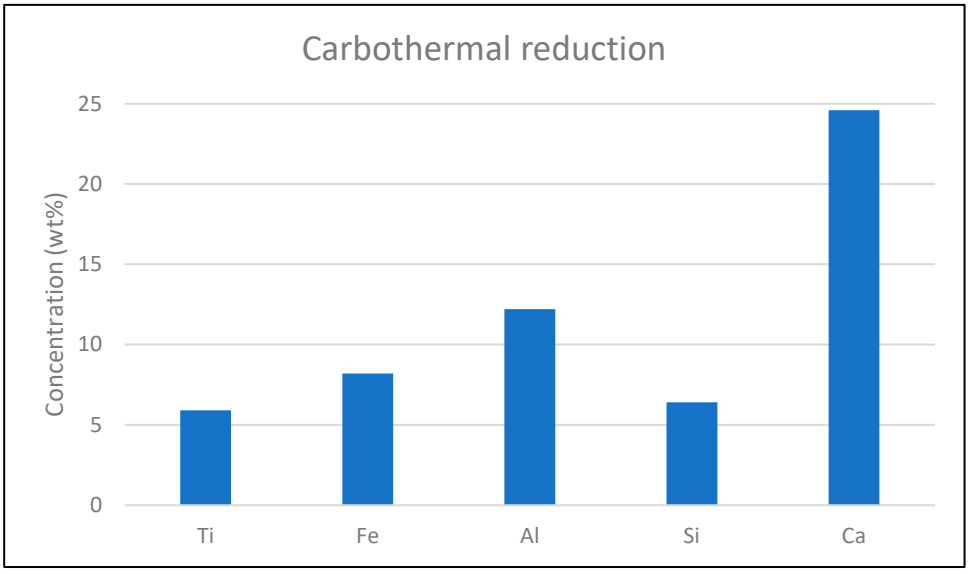


Figure 8. Elemental analysis of carbothermal-reduced slag at 1600 °C.

This Figure 8 shows the results of ICP analysis and composition (in weight percentage, wt%) of various elements, such as iron (Fe), titanium (Ti), silicon (Si), aluminum (Al), and calcium (Ca), in the slag after carbothermal reduction. The high concentration of calcium, approaching 30%, reflects the addition of CaO as a flux agent during the process. Compared to the original red mud, which contained a very low amount of calcium, the introduction of CaO significantly increases its concentration in the reduced slag. Aluminum also shows

an increase in concentration, slightly above 10%. The concentration of iron is reduced to between 10% and, 5%, representing a successful reduction of iron oxides. Silicon and titanium are also significantly enriched in slag due to the inertness of this reducing agent. This figure highlights the impact of adding CaO as a flux agent, showing that it became dominant in the slag.

Reduced red mud powder samples were analyzed at room temperature by the X-ray powder diffraction technique. All obtained powders were identified using the ICDD database at https://www.icdd.com (accessed on 20 March 2025).

The X-ray diffraction (XRD) results of the carbothermic reduction of red mud show (Figure 9) that hematite, boehmite, diaspore, ilmenite, perovskite, quartz, and other minerals have been transformed. XRD patterns of red mud (Figure 1) show characteristic peaks attributed to these phases, with hematite being a major component due to its high iron content. Aluminum-bearing phases, boehmite, diaspore, and titanium-containing minerals (ilmenite and perovskite) are also present in red mud along with quartz, which is a very common silicate phase.

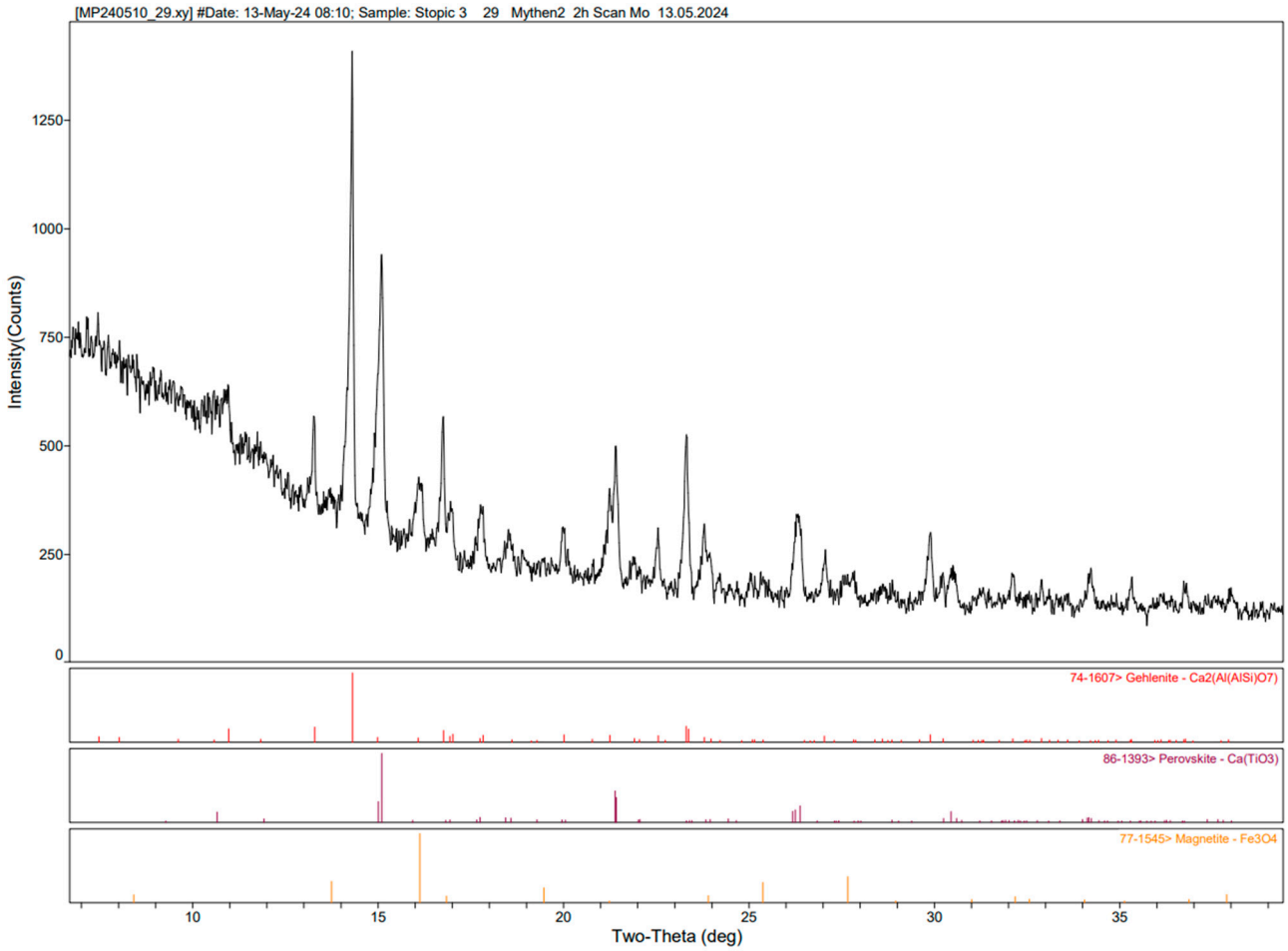


Figure 9. Diffractogram for slag obtained during red mud reduction at 1600 °C.

After the carbothermic reduction process, the XRD results are completely different. Hematite is no longer present because of its complete transformation. The reduction process produced two different phases: metallic (iron (Fe)) and slag. The XRD pattern of slag reveals the presence of perovskite, indicating that it remains largely unchanged, with the formation of gehlenite (calcium aluminum silicate) produced likely from the interaction of alumina with silica at high temperatures.

The absence of hematite peaks in the XRD pattern confirms its complete reduction, while the presence of magnetite suggests that some iron remained oxidized within the slag. The presence of perovskite indicates that titanium cannot be reduced, while the appearance of gehlenite reflects the complex transformations between the various oxides in red mud during the high-temperature exposure. Overall, the XRD results show the complete transformation of the red mud from a complex mixture of oxides and silicates to a system dominated by metallic iron and a slag phase, where perovskite and gehlenite are primary phases, with a minor amount of magnetite also present.

3.4. Hydrogen Reduction in the Rotary Kiln

After the reduction process, the quartz tube has been removed from the rotary kiln, and the obtained powder has been analyzed.

The XRD analysis of the sample revealed three distinct phases: Fe, perovskite, and gehlenite (Figure 10). This result is from the reduction of red mud with hydrogen, where hematite, the main phase in red mud, has been reduced. The formation of new phases, such as perovskite and gehlenite, indicate successful transformation during the reduction process, highlighting the potential of this method for modifying red mud and creating valuable materials. A total of 24.65% of mass loss for red mud has been achieved during the reduction, including a 10% loss of ignition. This means that 14.65% has been attributed to the reduction process of removing oxygen from iron in the form of water vapor.

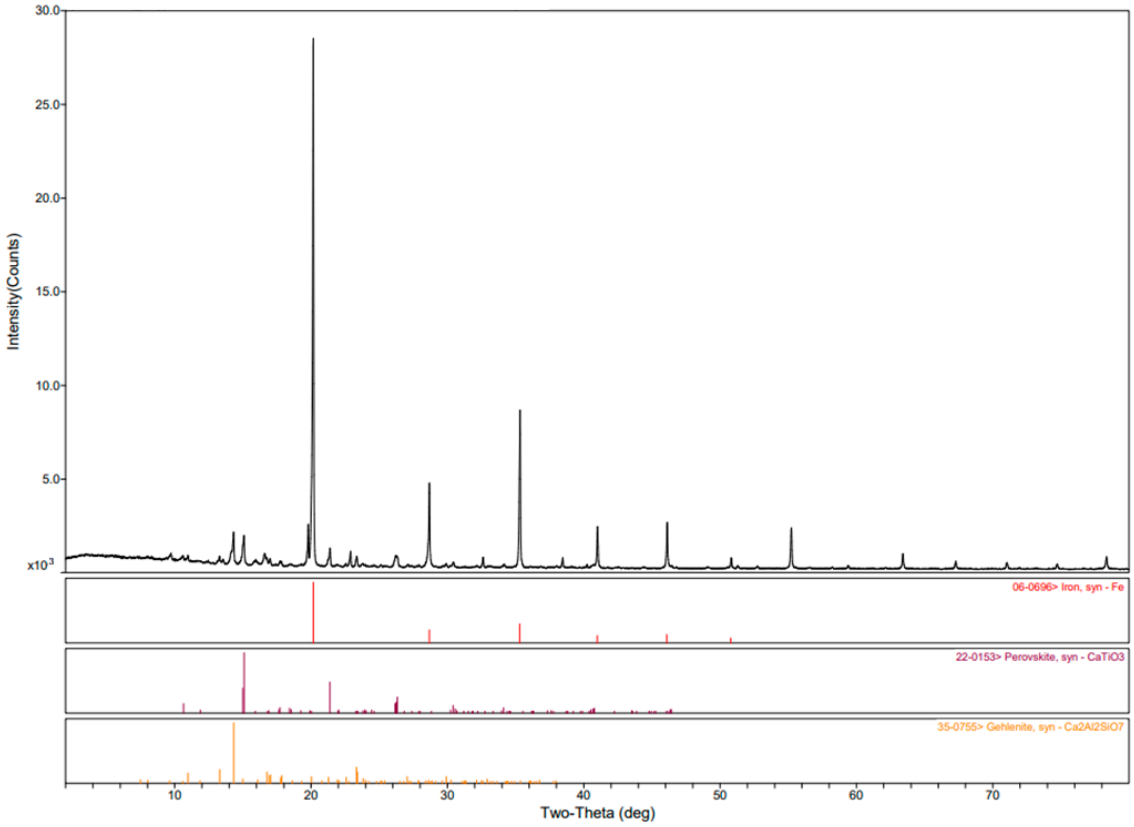


Figure 10. XRD analysis of hydrogen-reduced red mud.

3.5. Hydrogen Reduction in the Tubular Furnace

The prepared powders obtained between 800 °C and 1000 °C have irregular, polygonal forms with particle sizes of more than 100 µm, as shown in Figure 11a,b.

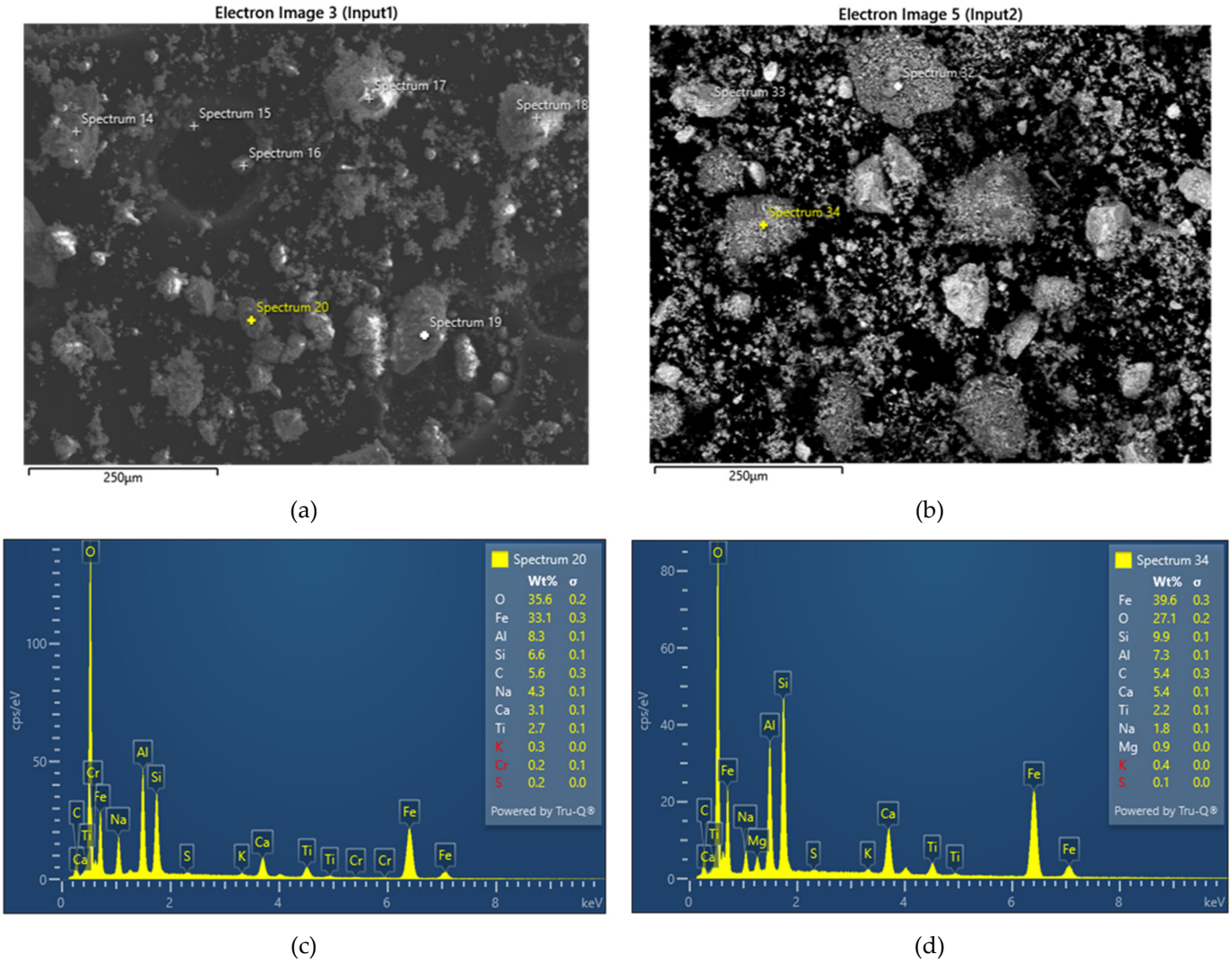


Figure 11. (**a**) SEM-Analysis of powder obtained by a hydrogen reduction of red mud at 800 °C; (**b**) SEM-Analysis of powder obtained by a hydrogen reduction of red mud at 1000 °C; (**c**) EDS-Analysis of powder obtained by a hydrogen reduction of red mud at 800 °C; (**d**) EDS-Analysis of powder obtained by a hydrogen reduction of red mud at 1000 °C.

An increase in temperature from 800 °C to 1000 °C increases the content of iron and decreases the content of oxygen, as shown in Figure 5. The morphological study of the reduced samples of iron oxides by H_2 shows agglomeration of the reaction product at temperatures between 800 and 1000 °C (Figure 11a,b).

The weight loss rate was calculated to indicate the degree of ilmenite hydrogen reduction. It was calculated as follows:

$$\alpha = (m_o - m_1/m_0) \times 100\% \quad (10)$$

where "α" denotes the weight loss ratio and "m_0" and "m_1" represent the mass before and after the hydrogen reaction, respectively.

The calculated mass loss of the initial sample amounted between 21 and 25% (as shown in Table 4), which is according to the expected total theoretical value of the reduction process regarding the mass loss of oxygen from iron oxide, cobalt oxide, and nickel oxide through hydrogen reduction (max 15%) and evaporation in the neutral atmosphere (max

10%). The obtained particles after hydrogen reduction have magnetic properties, which is very important for the following separation process.

Table 4. The experimental results for the reduction mass loss of red mud in a hydrogen atmosphere.

Mass Loss (%)	800 °C	900 °C	1000 °C
60 min	21	23	25

Diffractograms for three red mud samples reduced in a hydrogen atmosphere at 800, 900, and 1000 °C are shown in Figure 12. The identified phases include metallic iron, magnetite, perovskite, nepheline, and cancrinite.

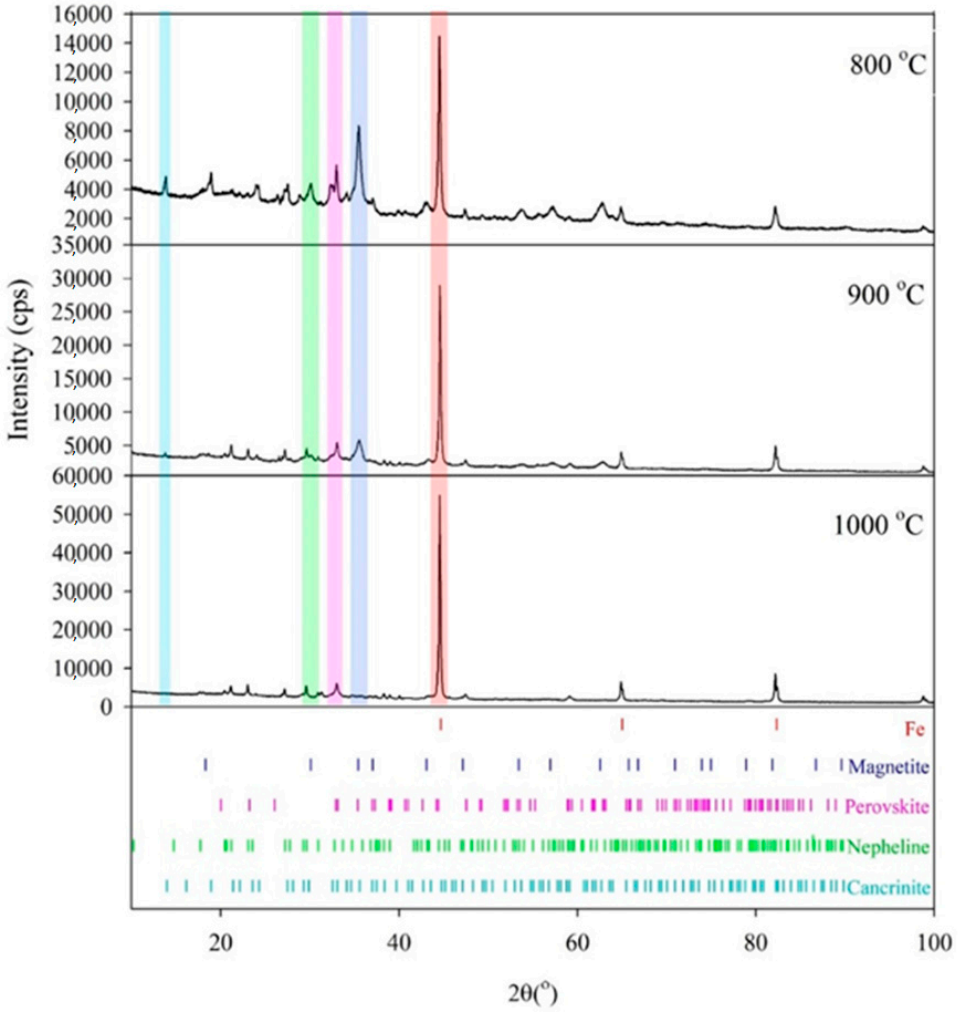


Figure 12. XRD analysis of the red mud reduced at 800, 900, and 1000 °C.

Metallic iron appears as a new phase not present in raw red mud, and it is characterized by a sharp diffraction peak that reflects the high crystallinity of iron. The intensities of iron diffraction peaks relative to those of other phases progressively increase with the reduction temperature, indicating an increase in iron abundance. At 900 °C, and especially at 1000 °C, metallic iron becomes the dominant phase.

Iron is partially present in magnetite, which is the most abundant phase in the sample reduced at 800 °C. The intensity of magnetite diffraction peaks and their content progressively decrease with increasing reduction temperature. A change in the position of the diffraction maxima compared to pure Fe_3O_4 may be attributed to the presence of Al, Ti, and Ca, which is consistent with the presence of these alloying elements, as determined

by EDS analysis. A notable feature is the progressive increase in metallic iron content accompanied by a decrease in magnetite content with increasing reduction temperature. Magnetite is virtually absent in the sample reduced at 1000 °C, where only reduced elemental iron dominates.

Other non-ferrous phases identified include perovskite and nepheline, which are formed during the reduction process and are not present in the raw red mud, as well as residual cancrinite, which is present in raw red mud. Perovskite, the only Ti-bearing phase, appears to be stable across the examined temperature range (800–1000 °C), as inferred from XRD. Nepheline is the only formed silicate phase that is present in all products. The observed trend shows a decrease in residual cancrinite content accompanied by an increase in nepheline content with increasing reduction temperature, leading to the complete disappearance of cancrinite at the highest reduction temperature. This trend suggests the transformation of cancrinite into nepheline.

3.6. Hydrogen Plasma Reduction in the Electric Arc Furnace

The plasma-thermal reduction was carried out in a reduction furnace at the Max Planck Institute for Sustainable Materials. It is performed using hydrogen plasma instead of molecular hydrogen, carbon, or carbon monoxide as the reducing agent.

After the reduction, the metal phase was separated from the slag using a magnet. Both phases were weighed, and the mass balance shown in Figure 13 was created. Since the metal phase was deposited in small droplets, it is possible that tiny metal droplets, invisible to the naked eye, remained in the slag phase. At the same time, small amounts of slag could adhere to the metal phase, leading to errors in the mass balance. Additionally, losses may occur during the handling of the samples.

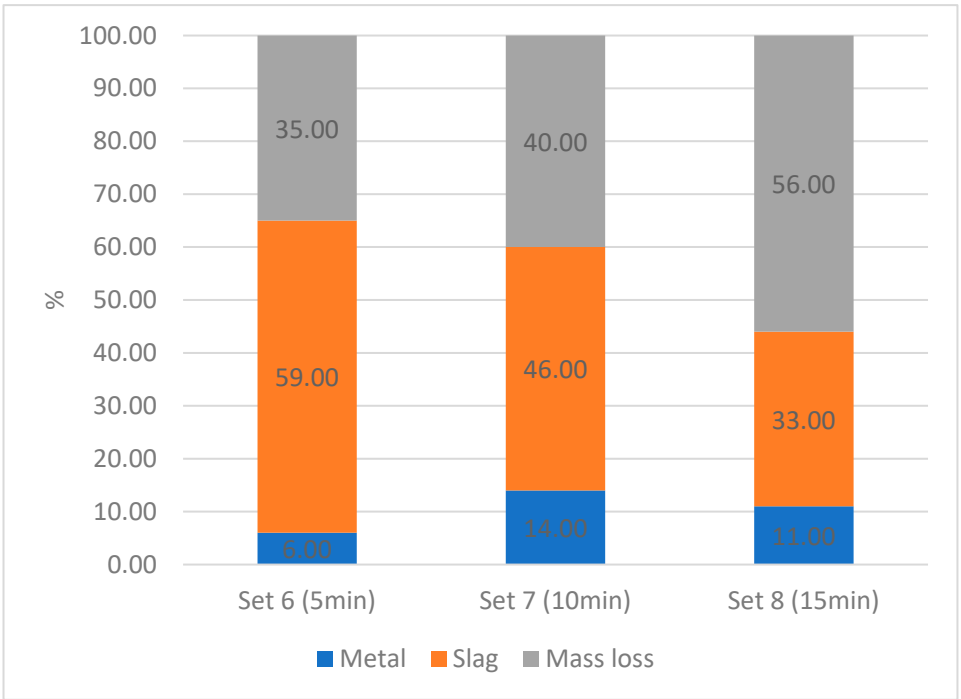


Figure 13. Mass balance of H-plasma reduction.

Figure 13 illustrates the mass balance observed during the plasma-thermal reduction process. Mass losses of up to 56% were achieved, a portion of which could be attributed to the reduction of oxides to metals, primarily aiming to produce a metallic iron phase and remove iron from the slag. However, analysis indicates that a significant part of the mass loss is not solely due to the reduction reaction but may also be caused by other factors,

like moisture in the feed material, losses during handling, and dust or evaporation during the experiment. Figure 13 shows the highest amount of the metallic phase obtained with a 10 min reaction time, suggesting that it can be optimal for these parameters. The various results in mass loss for different experiments indicate potential dependence on unknown factors, like parameter fluctuations or inhomogeneous feed material.

Figure 14 shows the results of the XRD analysis of plasma-reduced red mud. It shows characteristic peaks for different compounds, and it can be seen that hematite is completely reduced to either magnetite and wustite or metallic iron. The analysis also detects iron titanium oxide ($FeTiO_3$) known as ilmenite, which is a primary mineral used for titanium extraction. As XRD analysis only identifies compounds in a crystalline structure, only silicon oxide (cristobalite) was identified, while the remaining components, like aluminum and calcium, detected by ICP, do not appear in the XRD analysis. This absence suggests that these elements are likely present in an amorphous phase, which cannot be detected by XRD. Agrawal [33] mentioned that gibbsite from red mud was dexydroxylated to alumina during hydrogen reduction at higher temperatures (750–900 °C). But, the transformation in hydrogen plasma conditions in a short time above 1800 °C shall be investigated in detail using quantitative XRD analysis.

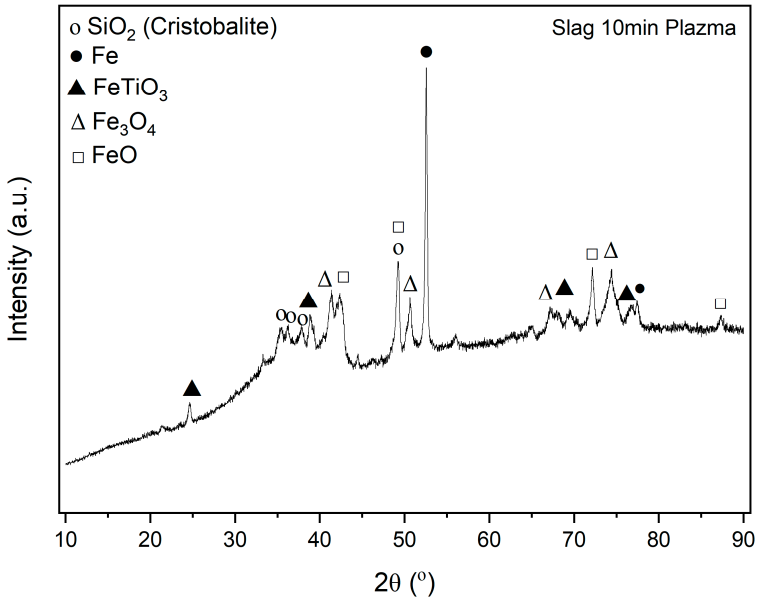


Figure 14. XRD analysis of a plasma thermally reduced red mud slag after 10 min of reduction time.

Figure 14 shows the limitations of XRD in making quantitative assessments, as it cannot determine all the elements that are present in the sample. Comparative analysis confirms that the reduction process has high significance in leaching efficiency, as shown in Table 5.

Table 5. Comparative analysis of the reduction process and leaching efficiency of solid residue (150°C, s/L: 1:10; 1 h, 500 rpm, pH < 0).

Reduction	Rotary Kiln (H_2)	Electric Arc Furnace (H)	Electric Arc Furnace (C) [26]
Content of iron in solid residue (%)	30	23	8
Leaching efficiency at 150 °C (%)	99	86	96

A reduction in all cases produces a product with magnetic properties. The obtained results confirmed that the reduction efficiency with carbon is highest, but it takes more time

(2 h) to produce titanium carbide and carbon dioxide, which is not environmentally friendly. The use of decarbonizing technology with plasma hydrogen in a short time (10 min) and with only 10% H_2 in the mixture can be optimized in order to produce metallic iron. But, the separation process of metallic iron by magnetic separation is most effective after hydrogen plasma reduction. The leaching efficiency is maximal for the solid residue after a reduction in the rotary furnace with hydrogen and in the electric arc furnace with carbon. The leaching efficiency of slag after hydrogen plasma reduction (86%) is higher than that in previous literature data, but it can be optimized through the reduction process in future research.

Maybe some pretreatment of red mud can increase reduction efficiency. Jena et al. [34] proposed a novel approach involving ultrasonication followed by water washing to pre-concentrate iron before reduction roasting of BR. Conventional reduction roasting of BR is more expensive compared to pre-concentrated BR, making this method potentially cost effective. The process consists of a two-stage ultrasonic treatment procedure. In the first stage, ultrasonication at 30 °C, with 40% solid content (w/v) for 30 min, improves the iron grade to 41.2 wt. (%) with 82% recovery. However, a second stage of ultrasonication is necessary to further upgrade the iron. Although the study optimized the ultrasonication time, temperature, solid content (%, w/v), and water washing parameters, an application in scale-up conditions shall be studied in detail using red mud from Alumina, Bosnia.

4. Conclusions

This study investigated the reduction of iron oxides from red mud using both carbothermal and hydrogen-based reduction methods, combining thermochemical modeling and experimental validation.

Thermochemical calculations provided insights into the reduction mechanisms of red mud. In the carbothermal reduction model, Fe_2O_3 was initially reduced to FeO before further transforming into metallic iron. The process was strongly influenced by carbon mass, with an optimal range between 10 g and 15 g to maximize metal recovery while minimizing impurity incorporation. Temperature had a moderate impact, with 1700 °C showing slightly improved metal yield. Similarly, the hydrogen reduction model indicated that Fe_2O_3 first converts into FeO before reducing to metallic iron, with 20 g of hydrogen identified as the optimal amount for effective reduction. Hydrogen reduction resulted in significantly purer iron compared to carbothermal reduction, with minimal impurity incorporation.

Experimental carbothermal reduction confirmed the thermochemical modeling results, with iron successfully extracted while impurities, such as silicon and titanium, remained in the slag. The addition of CaO as a flux agent significantly increased the calcium content in the slag. X-ray diffraction (XRD) analysis confirmed complete hematite reduction, resulting in metallic iron and a slag phase dominated by perovskite and gehlenite. Some magnetite remained in the slag, indicating an incomplete reduction of iron oxides.

Hydrogen-based reduction was explored using three different approaches: a tubular furnace, a rotary kiln, and hydrogen plasma reduction. In the tubular furnace, increasing the temperature from 800 °C to 1000 °C enhanced iron reduction, with iron purity increasing as oxygen content decreased. XRD confirmed the transformation of iron oxides into metallic iron, with residual magnetite decreasing at higher temperatures. The presence of perovskite and nepheline suggested interactions between alumina, silica, and titanium-bearing phases. Reduction in a rotary kiln resulted in a 24.65% mass loss, primarily due to oxygen removal in the form of water vapor. The process effectively converted hematite into metallic iron, with the presence of perovskite and gehlenite indicating phase transformations during reduction. Hydrogen plasma reduction achieved the highest mass loss, up to 56%, attributed to the reduction of oxides and process-related factors, such as evaporation and sample handling. The iron content in the slag significantly decreased, confirming the efficiency of plasma

reduction for iron extraction. XRD analysis identified iron titanium oxide (ilmenite) and suggested the presence of amorphous aluminum and calcium phases.

Both carbothermal and hydrogen-based reduction methods demonstrated effective iron recovery from red mud. Hydrogen reduction methods produced higher-purity iron, with the plasma process achieving the most significant reduction. The carbothermal reduction was more efficient in terms of overall metal yield but introduced more impurities. Among hydrogen-based techniques, plasma reduction achieved the highest iron extraction efficiency, while reduction in a tubular furnace and a rotary kiln provided scalable alternatives with good iron purity. These findings highlight the potential for hydrogen-based reduction as a cleaner alternative for iron recovery from red mud while also emphasizing the importance of optimizing parameters to balance yield and purity.

Author Contributions: Conceptualization, S.S. and D.K.; methodology, S.S.; software, A.M. and R.S.; validation, S.S., D.K. and I.R.S.F.; formal analysis, R.S. and I.R.S.F.; investigation, I.R.S.F., M.P. and D.K.; resources, S.S.; data curation, S.S.; writing—original draft preparation, D.K. and S.S.; writing—review and editing, I.R.S.F., M.P. and A.M.; visualization, D.K. and A.M.; supervision, B.F. and M.P.; project administration, S.S.; funding acquisition, S.S. and M.P. All authors have read and agreed to the published version of the manuscript.

Funding: This research was funded by the European Commission, grant number 101135077 (EURO-TITAN project).

Data Availability Statement: Data are contained within the article.

Conflicts of Interest: The authors declare no conflicts of interest.

References

1. Spreitzer, D.; Schenk, J. Reduction of Iron Oxides with Hydrogen—A Review. *Steel Res. Int.* **2019**, *90*, 1900108. [CrossRef]
2. Tokumitsu, K. Reduction of Metal Oxides by Mechanical Alloying Method. *Solid State Ion.* **1997**, *101–103*, 25–31. [CrossRef]
3. Rukini, A.; Rhamdhani, M.A.; Brooks, G.A.; Van den Bulck, A. Metals Production and Metal Oxides Reduction Using Hydrogen: A Review. *J. Sustain. Metall.* **2022**, *8*, 1–24. [CrossRef]
4. The Thermite Reaction Between Aluminium and Iron (III) Oxide | Experiment | RSC Education. Available online: https://edu.rsc.org/experiments/the-thermite-reaction-between-aluminium-and-ironiii-oxide/724.article (accessed on 23 July 2024).
5. Cheema, H.A.; Ilyas, S.; Farhan, M.; Yang, J.-H.; Kim, H. Extraction of Fe and Al from Red Mud Using Carbothermic Reduction Followed by Water Leaching. *J. Ind. Eng. Chem.* **2024**, *136*, 201–210. [CrossRef]
6. Blast Furnace Process—Tec-Science. Available online: https://www.tec-science.com/material-science/steel-making/blast-furnace-process/ (accessed on 23 July 2024).
7. Habibi, H.; Piruzian, D.; Shakibania, S.; Pourkarimi, Z.; Mokmeli, M. The Effect of Carbothermal Reduction on the Physical and Chemical Separation of the Red Mud Components. *Miner. Eng.* **2021**, *173*, 107216. [CrossRef]
8. Zinoveev, D.; Pasechnik, L.; Grudinsky, P.; Yurtaeva, A.; Dyubanov, V. Kinetics and Mechanism of Red Mud Carbothermic Reduction and Reduced Iron Grain Growth: An Influence of Sodium Sulfate. *Crystals* **2023**, *13*, 1. [CrossRef]
9. Lackner, A.; Molinari, T.; Paschen, P. A thermogravimetric study on the hydrogen reduction of tungsten oxides. *Scand. J. Metall.* **1996**, *25*, 115–121.
10. European Commision. A Roadmap for Moving to a Competitive Low-Carbon Economy in 2050—European Environment Agency. Available online: https://www.eea.europa.eu/policy-documents/com-2011-112-a-roadmap (accessed on 21 July 2024).
11. Cavaliere, P. Clean Ironmaking and Steelmaking Processes: Efficient Technologies for Greenhouse Emissions Abatement. In *Clean Ironmaking and Steelmaking Processes*; Springer: Cham, Switzerland, 2019; pp. 1–37.
12. Otto, A.; Robinius, M.; Grube, T.; Schiebahn, S.; Praktiknjo, A.; Stolten, D. Power-to-Steel: Reducing CO_2 through the Integration of Renewable Energy and Hydrogen into the German Steel Industry. *Energies* **2017**, *10*, 451. [CrossRef]
13. Souza Filho, I.R.; Ma, Y.; Kulse, M.; Ponge, D.; Gault, B.; Springer, H.; Raabe, D. Sustainable Steel through Hydrogen Plasma Reduction of Iron Ore: Process, Kinetics, Microstructure, Chemistry. *Acta Mater.* **2021**, *213*, 116971. [CrossRef]
14. Raabe, D. The Materials Science behind Sustainable Metals and Alloys. *Chem. Rev.* **2023**, *123*, 2436–2608. [CrossRef]
15. Souza Filho, I.R.; Springer, H.; Ma, Y.; Mahajan, A.; da Silva, C.C.; Kulse, M.; Raabe, D. Green Steel at Its Crossroads: Hybrid Hydrogen-Based Reduction of Iron Ores. *J. Clean. Prod.* **2022**, *340*, 130805. [CrossRef]

16. Cavaliere, P. Hydrogen Plasma Reduction. In *Hydrogen Assisted Direct Reduction of Iron Oxides*; Springer: Cham, Switzerland, 2022; pp. 321–338.
17. Tang, W.; Khavarian, M.; Yousefi, A. Red Mud. Sustainable Concrete Made with Ashes and Dust from Different Sources. *Mater. Prop. Appl.* **2022**, 577–606.
18. Liu, Y.; Naidu, R. Hidden Values in Bauxite Residue (Red Mud): Recovery of Metals. *Waste Manag.* **2014**, *34*, 2662–2673. [CrossRef] [PubMed]
19. Qi, Y. The Neutralization and Recycling of Red Mud-a Review. *J. Phys. Conf. Ser.* **2021**, *1759*, 12004. [CrossRef]
20. Verma, A.S.; Suri, N.M.; Kant, S. Applications of Bauxite Residue: A Mini-Review. *Waste Manag. Res.* **2017**, *35*, 999–1012. [CrossRef]
21. Tanvar, H.; Merino, K.; Mishra, B. Extraction of High Purity Magnetite from Bauxite Residue. *Miner. Eng.* **2023**, *199*, 108131. [CrossRef]
22. Rai, S.; Bahadure, S.; Chaddha, M.J.; Agnihotri, A. Disposal Practices and Utilization of Red Mud (Bauxite Residue): A Review in Indian Context and Abroad. *J. Sustain. Metall.* **2020**, *6*, 1–8. [CrossRef]
23. Winkler, D.; Bidló, A.; Bolodár-Varga, B.; Erdő, Á.; Horváth, A. Long-Term Ecological Effects of the Red Mud Disaster in Hungary: Regeneration of Red Mud Flooded Areas in a Contaminated Industrial Region. *Sci. Total Environ.* **2018**, *644*, 1292–1303. [CrossRef]
24. FactSage Software and Databases. Available online: https://factsage.com/ (accessed on 6 March 2025).
25. Stopic, S.; Kostić, D.; Schneider, R.; Sievers, M.; Wegmann, F.; Emil Kaya, E.; Perušić, M.; Friedrich, B. Recovery of Titanium from Red Mud Using Carbothermic Reduction and High Pressure Leaching of the Slag in an Autoclave. *Minerals* **2024**, *14*, 1151. [CrossRef]
26. Menad, N.; Kanari, N. Recovery of high grade iron compounds from LD slag by enhanced magnetic separation techniques. *Int. J. Miner. Process.* **2014**, *126*, 1–9. [CrossRef]
27. Pineau, A.; Kanari, N.; Gaballah, I. Kinetics of Reduction of Iron Oxides by H_2: Part I: Low Temperature Reduction of Hematite. *Thermochim. Acta* **2006**, *447*, 89–100. [CrossRef]
28. Pilla, G.; Kapelari, S.V.; Hertel, T.; Blanpain, B.; Pontikes, Y. Hydrogen Reduction of Bauxite Residue and Selective Metal Recovery. *Mater. Today Proc.* **2022**, *57*, 705–710. [CrossRef]
29. Lazou, A.; van der Eijk, C.; Balomenos, E.; Kolbeinsen, L.; Safarian, J. On the Direct Reduction Phenomena of Bauxite Ore Using H_2 Gas in a Fixed Bed Reactor. *J. Sustain. Metall.* **2020**, *6*, 227–238. [CrossRef]
30. Taskinen, P.; Hytönen, P.; Tikkanen, H. On the Reduction of Tungsten Oxides, II. *Scand. J. Metall.* **1977**, *6*, 228–232.
31. Stopic, S.; Nikolić, N.; Životić, D.; Krstić, J.; Rosić, M.; Damjanović, V.; Friedrich, B. Hydrogen Metallurgy for a Treatment of Bauxite Residues-First Results on the EURO-TITAN Project. In Proceedings of the XXV YuCorr; Ministry of Science, Technological Development and Innovation of the Republic of Serbia, Divčibare, Serbia, 29 May 2024; pp. 11–20.
32. Balomenos, E.; Gianopoulou, I.; Panias, D.; Paspaliaris, I. ENEXAL: Novel technologies for enhanced energy and exergy efficiencies in primary aluminium production industry. *Metall. Mater. Eng.* **2009**, *15*, 203–217.
33. Agrawal, S.; Dhawan, N. Hydrogen Reduction of Red Mud for Extraction of Metallic Values. *J. Sustain. Metall.* **2023**, *9*, 386–397. [CrossRef]
34. Jena, S.; Nayak, A.; Das, S. Ultrasonic-assisted pre-concentration of iron values in bauxite residue suitable for reduction-roasting purpose. *Chem. Eng. Commun.* **2025**, *212*, 4. [CrossRef]

Disclaimer/Publisher's Note: The statements, opinions and data contained in all publications are solely those of the individual author(s) and contributor(s) and not of MDPI and/or the editor(s). MDPI and/or the editor(s) disclaim responsibility for any injury to people or property resulting from any ideas, methods, instructions or products referred to in the content.